

Highly conductive partially cross-linked poly(2,6-dimethyl-1,4-phenylene oxide) as anion exchange membrane and ionomer for water electrolysis

Zhiming Feng^a, Pilar Ocón Esteban^b, Gaurav Gupta^a, David A Fulton^c and Mohamed Mamlouk^{a}*

^aSchool of Engineering, Newcastle University, Merz Court, Newcastle upon Tyne, NE1 7RU, United Kingdom

^bDepartment of Physical Chemistry, University of Autonomo of Madrid, C/ Francisco Tomás y Valiente 7, 28049 Madrid, Spain

^cSchool of Natural and Environmental Sciences, Bedson Building, Newcastle University, Newcastle upon Tyne, NE1 7RU, United Kingdom

**corresponding author*

E-mail address: mohamed.mamlouk@newcastle.ac.uk (M. Mamlouk)

Abstract

Cross-linked quaternised Poly(2,6-dimethyl-1,4-Phenylene Oxide) (QPPO)-based membranes were prepared via Friedel-Crafts reactions using SnCl_4 catalyst, 1,3,5-trioxane and chlorotrimethylsilane as environmentally-friendly chloromethylating reagents. New equations to calculate the degree of chloromethylation (**DC**) and cross-linking degree (**CLD**) were proposed. Ionic conductivity of 133 mS cm^{-1} at $80 \text{ }^\circ\text{C}$ was obtained, one of the highest reported for QPPO based membranes. We have compared QPPO to chloromethylated polystyrene-b-poly(ethylene/butylene)-b-polystyrene (SEBS) ionomer and report on the importance of ionomer-membrane interaction as well as the trade-off between swelling ratio and conductivity on performance and mechanical stability of AEM water electrolyser. Exsitu stability testing after 500h in 1M KOH showed membranes retained up to 94% of their original **IEC**. QPPO was employed as both membranes and ionomers in electrolyser tests. QPPO membranes exhibited area specific resistance of $104 \text{ m}\Omega \text{ cm}^{-2}$ and electrolyser current density of 814 mA cm^{-2} at 2.0 V in 0.1M NaOH solution at $40 \text{ }^\circ\text{C}$.

Keywords: PPO, Poly(2,6-dimethyl-1,4-Phenylene Oxide), AEM, Friedel-Crafts reactions, water electrolyser

1. Introduction

Renewables hold the answer to the energy crisis. The increasing global energy demand is forecast to grow 58 % by 2040.[1, 2] Hydrogen is considered one of the most promising fuels or building blocks for the long term storage of renewable energy [3-5]. Water electrolyzers provide a high-efficiency and environmentally friendly method to produce green hydrogen.[6, 7] There are three main technologies for water electrolysis, namely, alkaline water electrolyser is (AWE), polymer electrolyte water electrolyser, and high-temperature solid oxide water electrolyser (HT-SOWE) [8]. AWEs are a mature technology and utilise the alkaline solution as the electrolyte. However, there are still some issues, such as the low current density, electrolyte corrosion, etc. HT-SOWEs are operated at a high temperature typically between 700 to 950 °C. This technology is in lab-scale. Polymer electrolyte water electrolyser includes proton exchange membrane water electrolyzers (PEMWEs) and anion exchange membrane water electrolyzers (AEMWEs). They are operated at ambient temperature from 50 to 80 °C. Compared with proton exchange membrane water electrolyzers (PEMWEs) [9-14], Anion Exchange Membrane Water Electrolyzers (AEMWEs) are at an early stage of development [3, 15, 16]. AEMWEs could provide an environment for faster oxygen evolution reaction kinetics, and allow for use of non-precious metal oxide catalysts at the anode, such as NiCo_2O_4 and MnO_2 . Additionally, stainless steel or Nickel based current collectors can be utilised, which will also decrease the cost of the device [17, 18].

Anion exchange membrane (AEM) is one of the key components in AEMWEs serving as hydroxide ion (OH^-) conductor and separator between hydrogen and oxygen gases [19, 20]. To ensure the high performance and operation efficiency of a water electrolyser, stringent requirements, including good thermal and mechanical stability, high ionic conductivity and

long-term chemical stability for the AEMs are needed [21, 22]. There are remaining challenges for AEM. According to the EU Horizon 2020/Fuel Cells and Hydrogen Joint Undertaking (JU), the ionic conductivity is expected to be higher than 50 mS cm^{-1} at room temperature. After 2000 h real or simulated operation, the area-specific resistance should be lower than $0.07 \text{ } \Omega \text{ cm}^2$ [23].

Poly(2,6-dimethyl-1,4-Phenylene Oxide) (PPO) is considered a good membrane candidate due to its excellent physicochemical properties, such as high transition temperature (T_g), excellent mechanical strength and good chemical stability [24-27]. PPO-based AEMs are usually prepared in three steps, namely, chloromethylation (or bromination), quaternisation and hydroxide ion exchange.[28] Among those steps, chloromethylation is crucial as it enables further PPO functionalization, which determines the functional groups of the polymer and influences the anion conductivity eventually. To chloromethylate PPO, Friedel-Crafts reaction plays a significant role. The conventional methods usually use ZnCl_2 or AlCl_3 as the Lewis acids catalyst and carcinogenic chemicals as chloromethylating reagents,[29] such as chloromethyl methyl ether (CMME) or bis-chloromethylether (BCME). Greener and more efficient chloromethylation methods have been researched, for example by using SnCl_4 as catalyst and paraformaldehyde ($(\text{HCHO})_n$) and chlorotrimethylsilane (TMCS) as chloromethylating reagents to replace the carcinogenic ones. Those new methods present an eco-friendly and simplified synthetic route for chloromethylation. Several studies employed this new method to chloromethylate the PPO. However, the ionic conductivity was too low for the cell operation [23] even under the high degree of chloromethylation,[30-33], which raised the need to further investigate the process of chloromethylation. Arges and co-workers [34] prepared PPO-based AEMs by using SnCl_4 as the catalyst. The ionic conductivity of the membrane in hydroxide form they obtained was 13 mS cm^{-1} at $30 \text{ }^\circ\text{C}$ with 13 % for the

degree of chloromethylation (DC). Becerra-Arciniegas and co-workers prepared PPO-based membrane with grafted trimethylammonium groups and the ionic conductivity in hydroxide form was 5.9 mS cm^{-1} at $60 \text{ }^\circ\text{C}$ with 54 % for DC. In addition to the low ionic conductivity, gelation was observed during the membrane preparation process, and the solvent extraction method was used to calculate the degree of gelation.[31] However, this method lacks high accuracy and has limited application, only suitable when the gel content is high enough to detect. We and others prepared chloromethylated polystyrene-*b*-poly (ethylene/ butylene)-*b*-polystyrene (SEBS) by using 1,3,5-trioxane to replace paraformaldehyde in the presence of SnCl_4 as catalyst [17, 35].

Given the research gap and previous studies, PPO-based AEMs and ionomer were prepared via Friedel-Crafts reactions using SnCl_4 as catalyst and 1,3,5-trioxane and chlorotrimethylsilane as chloromethylating reagents. Compared with other head groups, for instance, the imidazolium cation, benzyl ammonium provides relatively high ionic conductivity, acceptable stability and good environment (low adsorption on catalyst) [36]. For the performance of anion exchange membrane fuel cell, trimethylammonium (TMA) cation showed the highest power density than 1,2-dimethylimidazolium (DMIIm) and N-methylpiperidinium (Pip) cations [37]. Thus, benzyl ammonium is supposed to meet the requirement as the membrane is expected to be applied in water electrolyser when the working condition is close to a pH neutral environment or $\text{pH} < 14$ [38]. In addition, the steric hindrance of the crosslinking structure is expected to protect the benzyl ammonium group to some extent [36]. As a result, TMA was chosen as the cation. A variety of characterization techniques were used to measure ionic conductivity, thermal, mechanical and alkaline stabilities. The overlooked cross-linking side reaction was studied and explained. New and more accurate calculation methods for DC and cross-linking degree (CLD) were proposed.

Finally, in comparison with our previous studied membrane (low-density polyethylene, LDPE) [38] and ionomer (SEBS) [17], electrochemical testing with QPPO as both membrane and ionomer was done in electrolysis.

2. Experimental

2.1 Materials and methods

Poly(2,6-dimethyl-1,4-phenylene oxide) (PPO, product number 181781), *N*-methyl-2-pyrrolidinone (NMP), 1, 3, 5-trioxane, chlorotrimethylsilane (TMCS), SnCl₄ (product number 208930), chloroform, trimethylamine (TMA, in 45 % solution in H₂O), potassium hydroxide, methanol, sulphuric acid and sodium chloride were purchased from Sigma-Aldrich and used without further purification.

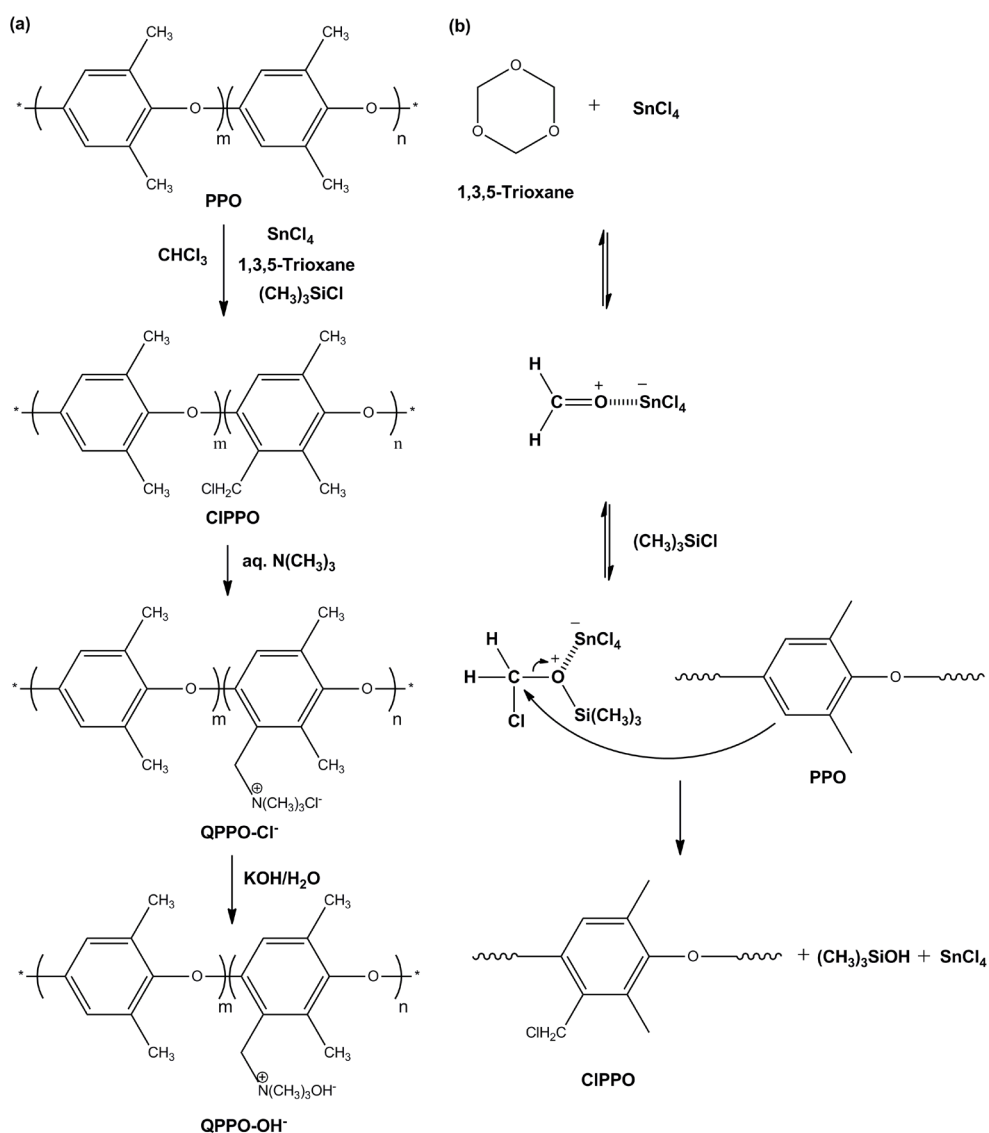


Fig. 1. (a) Synthetic route for PPO-based AEM. (b) Mechanism of chloromethylation of PPO.

As is shown in Fig. 1(a), the AEM was obtained through sequential chloromethylation, quaternisation and ion exchange steps. The mechanism of chloromethylation was shown in Fig. 1(b) [17, 39]. 1,3,5-trioxane undergoes a tautomeric process to form formaldehyde with protonation occurring in the presence of the SnCl_4 . Then, the intermediate with chlorotrimethylsilane and phenyl rings react. For example, unless otherwise specified, PPO (4.0 g) and chloroform (250 ml) were added into a three-neck round bottom flask fitted with a

reflux condenser under continuous nitrogen purging. After complete dissolution, 1,3,5-trioxane (1.7 g) and chlorotrimethylsilane (7.2 ml) were added. The SnCl_4 catalyst (0.8 ml) was injected into the flask with a syringe. The mixture was then stirred for 10 h at 35 °C. The chloromethylated PPO (CIPPO) was obtained after precipitation in methanol/water (150 ml/150 ml). CIPPO was purified by re-dissolution in chloroform and precipitated by methanol, then dried under vacuum (60 °C) overnight.

The process of quaternisation was done in a homogenous way, the polymer solution was prepared by dissolving CIPPO (120 mg) in NMP (4 ml). Quaternisation was performed by adding an appropriate amount of trimethylamine solution (45 wt % in water) into the mixture and allow 24 h at room temperature. The membranes were formed by casting the yellow transparent polymer solution onto a flat glass plate. After the solvent evaporated, the films were easily removed from the glass surface. The quaternised PPO (QPPO) membranes were obtained in chloride form (QPPO- Cl^-). To convert the (Cl^-) counter ion to hydroxide (OH^-), membranes were immersed into 1 M KOH solution for 1 h whilst changing the KOH solution every 20 min. The membrane films were then washed with de-ionized water several times to remove the excess KOH. Finally, the QPPO- OH^- was obtained (150~170 μm). The heterogeneous quaternisation was shown in the supporting information. 16 different QPPO-x (x:1-16) prepared from quaternising the corresponding CIPPO shown in Table S1.

2.2 Structure characterization

Fourier-transform infrared spectroscopy (FTIR) and nuclear magnetic resonance (NMR) were used to characterize the structure of the polymer. A Varian 800 FT-IR in Attenuated Total Reflectance (ATR) mode was used to verify the successful introduction of functional groups. Samples of PPO, CIPPO and QPPO were analysed by FTIR. ^1H NMR spectra of PPO and CIPPO were recorded on a Bruker Av-400-WB instrument using CDCl_3 as solvent [31]. The

scanning electron microscope (SEM) was employed to analyse the surface morphology of substance. A focused beam of electrons was shot from the SEM and interacted with specimen atoms, producing various signals that contain lots of information about the sample, such as the surface topography. SEM analysis was performed by using a Tescan Vega 3LMU machine. Transmission electron microscopy (TEM) characterization was conducted by using Hitachi HT7800 120kV TEM. The samples for the TEM test were obtained by immersing the membranes into 0.1 M tetrachloroplatinate ions (KPt₂Cl₄) solution for 48 h, then washed with abundant water and followed by drying at 80 at under vacuum for 12 h. Then the stained membrane was embedded in epoxy resin placed in the copper grid before the test.

2.3 Ion exchange capacity, water uptake, swelling ratio and hydration number

Ion exchange capacity (*IEC*) was calculated by measuring the amount of OH⁻ ions in NaCl solution exchanged from the membrane with acid-base titration with Methyl red as the indicator. Before titration, the membrane in hydroxide form was immersed in a known volume of 1 M NaCl solution for 24 h to liberate the hydroxide ions. Then, 10 ml of the solution was titrated with a known concentration of H₂SO₄ solution until colour change was observed. The measurement was repeated 3 times to get an average. The membrane was then washed thoroughly with deionized water (DI) to remove the excess salt on the surface of the membrane. Finally, the membrane was dried in the oven overnight at 60 °C and weighed. The *IEC* was calculated using the amount of OH⁻, divided by the weight of the dry membrane, which is shown in eq. 1.

$$IEC = \frac{2 \times V_{H_2SO_4} \times C_{H_2SO_4}}{W_{dry}} \quad (1)$$

Where the $V_{H_2SO_4}$ is the volume of H_2SO_4 solution consumed in the titration, $C_{H_2SO_4}$ is the concentration of H_2SO_4 solution and W_{dry} is the weight of the dry membrane.

Water uptake (**WU**), swelling ratio (**SR**) and hydration number (λ) were measured by calculating the change of membrane weight and dimension before and after hydration, respectively. The membrane in OH^- form was soaked in deionized water for 48 h at room temperature. Then, the surface of the wet membrane was wiped with tissue paper to remove the water on the surface and weighed immediately. The hydrated membrane was dried in the oven at 60 °C overnight. For the calculation of WU, eq. 2 was used.

$$WU = \frac{W_{wet} - W_{dry}}{W_{dry}} \times 100\% \quad (2)$$

Where W_{wet} and W_{dry} were the weight of wet and dry membrane, respectively.

SR was measured as the average swelling in width, length and thickness of the membrane before and after drying. This was measured by using eq. 3.

$$SR = \frac{D_{wet} - D_{dry}}{D_{dry}} \times 100\% \quad (3)$$

Where D_{wet} is the studied dimension of the wet membrane, such as width, length or thickness, and D_{dry} is the corresponding dimension after the membrane was dried.

The hydration number is the number of water molecules per functional group and it was calculated by using eq. 4.

$$\lambda = \frac{m_{H_2O}}{M_{H_2O} \times IEC} \times 1000 \quad (4)$$

Where λ is the hydration number (dimensionless), m_{H_2O} is water uptake (m_{H_2O} = the weight of wet film – the weight of dry film). M_{H_2O} is the molecular weight of water ($g \text{ mol}^{-1}$).

2.4 Thermal stability

Thermal stability of the PPO-based samples was measured by thermogravimetric analysis (TGA) and differential scanning calorimetric (DSC). TGA was performed on a Perkin Elmer, TGA 4000 instrument. The sample was heated from 50 °C to 650 °C with a heating rate of 10 °C/min under a nitrogen atmosphere. DSC was investigated under a nitrogen atmosphere using TA Instruments, Q20. The sample was heated from 50 °C to 350 °C in an open alumina pan with a heating speed of 10 °C/min under a nitrogen atmosphere.

2.5 Mechanical properties

Tensile testing of QPPO was performed using a Model-Tinius Olsen H25KS to obtain the stress-strain plot with a constant crosshead velocity of 2 mm min⁻¹ for all the tests.

2.6 Ionic conductivity and activation energy

The membrane through-plane conductivity was measured by using an in-house test cell with an electrode area of 1.77 cm². To avoid direct reaction with the CO₂ in the air, the membrane was kept submerged in deionised water while loaded in conductivity cell and was tested under N₂ atmosphere. The membrane was sandwiched between two gas diffusion layer carbon electrodes in the cell under 100 % relative humidity and elevated temperature, which was verified by temperature and humidity sensors, respectively. The ionic conductivity was calculated by using eq. 5.

$$\sigma = \frac{4L}{R(\pi d^2)} \quad (5)$$

Where σ is the hydroxide ionic conductivity, L is the membrane thickness, R is the resistance derived from the impedance value at a zero-phase angle, and d is the diameter of the actual testing area. The impedance was measured using the same procedure previously reported [38].

The activation energy (E_a) of ion transport is consistent with the energy barrier of anion migration [40]. E_a can be determined with the Arrhenium relationship between conductivity and temperature. The eq. 6 was as follows.

$$E_a = -b \times R_g \quad (6)$$

Where b is the slope of linear regression of $\ln\sigma$ versus $1000/T$, and R_g is the gas constant.

2.7 Alkaline stability

The alkaline stability of the membrane was measured by immersing the membrane in 1 M KOH solution at room temperature and 60 °C for 500 h. Then, the change of IEC and weight loss were calculated based on before and after alkaline treatment data.

2.8 Electrochemical measurements

The electrochemical performance of the membrane and the ionomer were tested in electrolyser cells by preparing a membrane electrolyte assembly (MEA) using Pt/C catalyst at the cathode (0.4 mg cm^{-2}) and NiCo_2O_4 at the anode (2 mg cm^{-2}) [17]. At the anode side, titanium fiber felt GDL with a thickness of 0.3 mm and 78% porosity (Bekaert Toko metal fiber Co., Ltd.) was used for oxygen evolution reaction. The anode catalyst ink, consisting of NiCo_2O_4 , 28 wt% ionomer and N-Methylpiperidine as the solvent, was sprayed on the Titanium GDL directly. As for the hydrogen evolution reaction electrode, non-wet-proofed carbon GDL with MPL (product code H2315 C9, Freudenberg Germany) was used. The catalyst at the cathode was 20% Pt/ C, 28 wt% ionomer and isopropanol. PPO membrane and ionomers synthesised in the current study were compared against bench-mark LDPE based AEM and SEBS ionomer reported previously [17, 41]. Autolab potentiostats instrument (PGSTAT302 N) was used to conduct the electrochemical analysis. Cyclic voltammetry studies were done by cycling between 1.3 to 2 V at a scan rate of 1 mV s^{-1} and the

electrochemical impedance spectroscopy was done at 1.7 V. The experiments were operated by circulating 0.1 M NaOH to both anode and cathode at 40 °C.

3. Results and discussion

3.1 FTIR spectroscopy

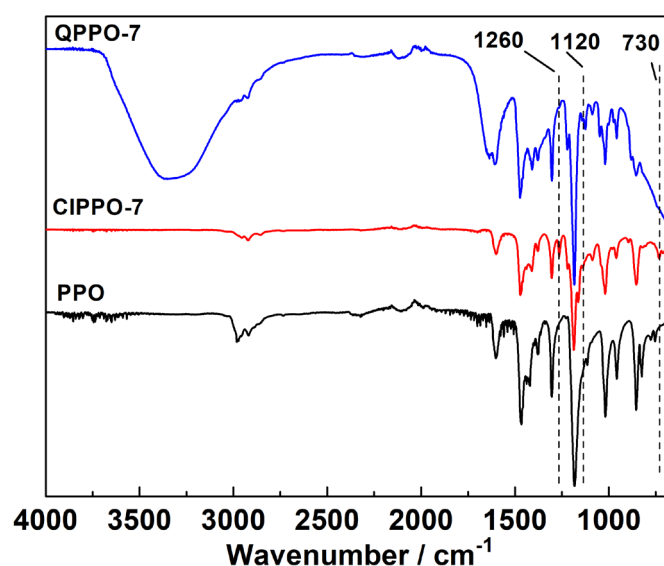


Fig. 2. FTIR spectroscopic comparison of QPPO-7, CIPPO-7 and PPO.

Fig. 2 shows the FTIR spectra of pristine PPO, CIPPO, and QPPO collected in the ATR mode. QPPO-7 and CIPPO-7 were tested. The signals at 1600 cm^{-1} and 1189 cm^{-1} were assigned to C=C bonds stretching in aromatic rings and C-O-C stretching, respectively and is that of the polymer backbone [42]. After chloromethylation, new peaks at 1260 cm^{-1} and 730 cm^{-1} were assigned to the C-Cl bonds [43], confirming the successful chloromethylation of the polymer. The broad bands at 3380 cm^{-2} were assigned to the stretching vibration of O-H bands in water. Furthermore, a new peak at 1120 cm^{-1} observed after quaternisation was assigned to the C-N vibration[29], indicating the successful introduction of the quaternary ammonium group [43].

3.2 ^1H and ^{13}C NMR

^1H and ^{13}C NMR spectroscopy were used to confirm the structure of CIPPO and calculate the degree of chloromethylation. Fig. 3(a) shows the ^1H NMR spectra of pristine PPO (bottom),

partially chloromethylated PPO (middle) and fully chloromethylated PPO (top). Taking partially chloromethylated PPO as an example, additional signals in the spectra in comparison with pristine PPO can be seen. The signal at $\delta = 6.5$ ppm corresponds to the aryl proton of PPO (labeled as *a*). Due to the electrophilic substitution, some aryl protons are shifted to $\delta = 6.1$ ppm (labeled as *d*). The signal at $\delta = 5$ ppm was assigned to the chloromethyl group (labeled as *c*), which confirms the chloromethylation. Owing to the deactivating effect of the chloromethyl group, mono-chloromethyl substituted aromatic compounds are obtained [32, 44, 45]. The signal at $\delta = 2.0$ ppm was assigned to the methyl groups. Due to changes in its chemical environment and the effect of surrounding protons, the chemical shift and multiplicities of ClPPO were different from those of pristine PPO. To make it clearer in the following explanation, protons in the methyl groups were labeled as *b*, *b'* & *b''* (Fig 3(a)).

3.3 Cross-linking during chloromethylation

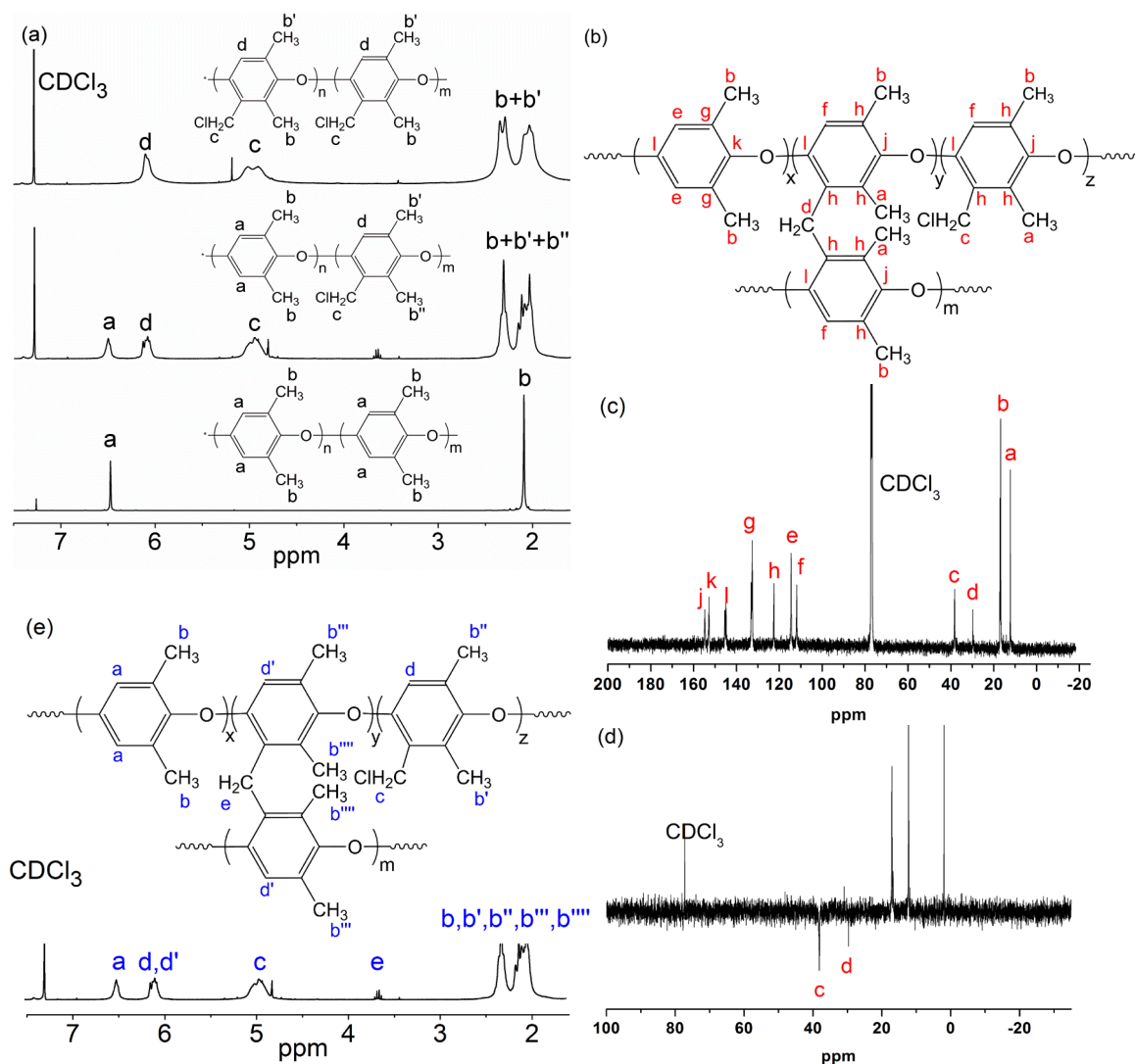


Fig. 3. (a) ¹H NMR spectra of pure PPO (bottom), partially chloromethylated PPO (middle, CIPPO-5) and fully chloromethylated PPO (top, CIPPO-1) (CDCl₃, 400 MHz). (b) The proposed cross-linked structure of CIPPO-5. (c) ¹³C NMR (CDCl₃, 100MHz) of (b). (d) ¹³C NMR DEPT 135 spectra of (b). (e) the ¹H NMR spectra of cross-linked CIPPO-5.

The degree of chloromethylation (*DC*) was one of the significant parameters to characterize the degree of functionalization and has a significant effect on membrane performance. To the best of our knowledge, nearly all the reported literature calculated *DC* by using eq. (7) [31, 43, 46, 47].

$$DC_1(\%) = \frac{A(H_d)}{0.5A(H_a)+A(H_d)} \times 100 \quad (7)$$

A: The integrated area of the proton signal in the ^1H NMR spectra.

As is shown in Fig. 3(a), once chloromethylation occurs, the chemical shift at position *d* changes from $\delta = 6.5$ ppm to $\delta = 6.1$ ppm. Thus, the area of protons (AP) at position *d* can be used to characterize the degree of chloromethylation.

Apart from eq. (7), Manohar and co-workers used eq. (8), which uses a similar method and will be discussed in the following section. [33]

$$DC'(\%) = \frac{2A(H_c)}{A(H_d)} \times 100 \quad (8)$$

A: The integrated area of the proton signal in the ^1H NMR spectra.

Table S1 shows the degree of chloromethylation (error $\pm 5\%$) of CIPPO obtained under different experimental conditions, such as temperature, the ratio between reactants and catalyst, reaction time and the concentration of reactants. Theoretically, once the chloromethylation reaction occurs, the signals for H_d and H_c should appear simultaneously and the integration of H_d peak i.e. $A(H_d)$, should be half of that of H_c since the amount of hydrogen at position *c* is twice as much as that at position *d* i.e. $A(H_d)/A(H_c) = 0.5$. However, as is shown in table S1, the ratios of $A(H_d)$ and $A(H_c)$ are not 0.5 for all prepared CIPPO samples, which suggests that there is a side reaction occurring.

In fact, in the case of PPO, the alkylation would result in the linking of two aromatic rings with methylene bridge under Lewis acid environment (SnCl_4) and produce a cross-linked PPO structure. This is also reported for other polymers such as polystyrene [48, 49]. As is shown in Fig. 4, there appears to be a competition between the chloromethylation reaction (Route A) and the cross-linking reaction (Route B). The side reaction between the chloromethyl groups and the aromatic rings should be considered. Therefore, we proposed a

cross-linked polymer structure after chloromethylation in Fig 3(b) and the cross-linking process route B as shown in Fig. 4.

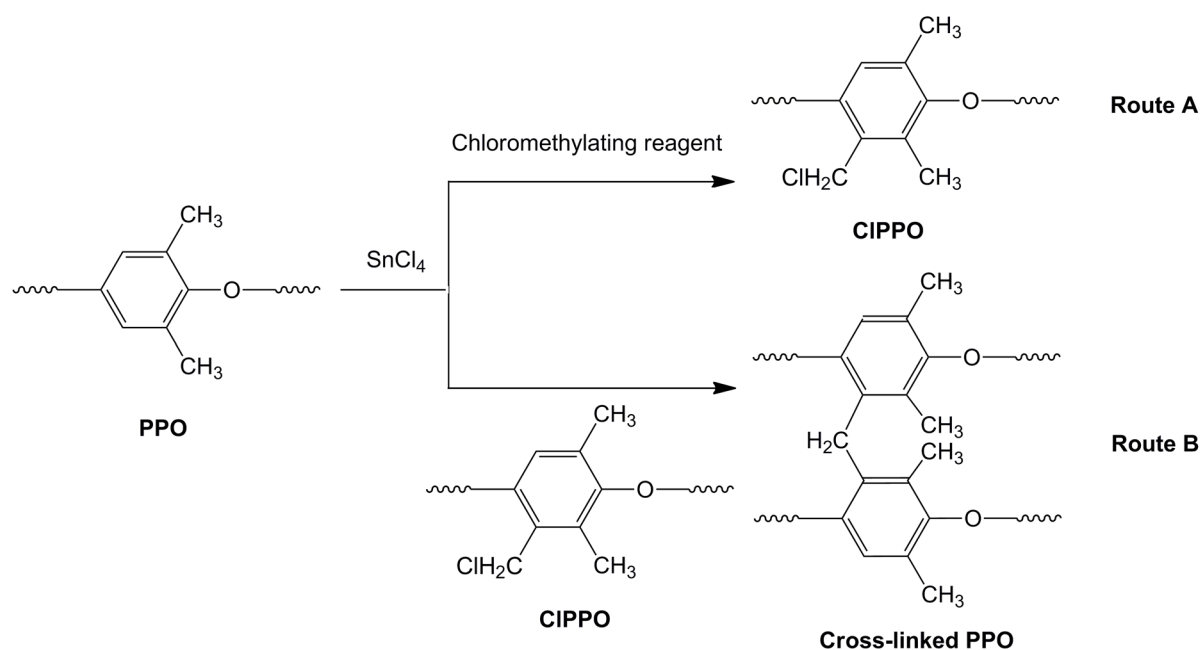


Fig. 4. The competition between chloromethylating reagent and substituted benzyl chloride for unsubstituted PPO.

The proposed cross-linking structure was verified by ^{13}C NMR spectra, as is shown in Fig. 3(c). The signal at $\delta = 29.71$ ppm corresponds to the methylene carbon (position *d*) in Fig. 3(b) confirming the presence of cross-linking, and the signal at $\delta = 38.27$ ppm corresponds to the chloromethyl carbon (position *c*) confirming the polymer chloromethylation [50, 51]. In order to verify the proposed cross-linked polymer structure further, ^{13}C NMR DEPT 135 spectroscopy of CIPPO was conducted. With this technique, CH and CH_3 carbon atoms appear as positive signals and CH_2 one appears as negative signals and quaternary carbon atoms do not show any signal. As is shown in Fig. 3(d), two signals ($\delta = 29.71$ ppm and $\delta = 38.37$ ppm) appear under X-axis, which corresponds to methylene carbon and chloromethyl carbon, respectively, confirming the proposed cross-linking structure.

As is shown in Fig. 4, chloromethylation and cross-linking are competitive reactions even though cross-linking only occurs after chloromethylation reaction. These two reactions occur at the same benzene ring (position *a*). At a short reaction time, the chloromethylation reaction is very fast and will be the dominant reaction as the number of available aromatic rings is high, with an increase of reaction time and increase in substituted aromatic rings and decrease in aromatic rings available for substitution cross-linking reaction dominates.

Therefore, we re-analyse the ¹H NMR in Fig. 3(e). Taking partially chloromethylated PPO as an example, after chloromethylation, the area of protons (AP) at position *c* should be twice as that at position *d*. Once cross-linking occurs, one methylene group will be generated and connected to two benzene rings. Thus, the AP at position *e* should be equal to that at position *d'*. Furthermore, the AP at position *c* or *d* can thus be used to estimate the unreacted chloromethyl groups, which corresponds to the practical degree of chloromethylation after cross-linking. The AP at position *d'* or *e* can be used to estimate the number of methylene groups, as well as the cross-linking degree. However, the protons at positions *d* and *d'* have similar chemical shifts (ca. 6.1 ppm), which makes it difficult to distinguish between the two and to determine the degree of cross-linking. Therefore, when calculating the degree of chloromethylation, the protons at position *c* should be considered. Thus, a new equation has been proposed here using the ratio among $A(H_c)$, $A(H_a)$, $A(H_d)$ and $A(H_{d'})$ as eq. (9), (designated as DC_2).

$$DC_2(\%) = \frac{0.5A(H_c)}{0.5A(H_a)+A(H_d)+A(H_{d'})} \times 100 \quad (9)$$

$A(H_d)$ plus $A(H_{d'})$ equals $A(H_d, H_{d'})$ which can be used to instead $A(H_d)$ and $A(H_{d'})$. As discussed above, the generation of the methylene bridge (position *e*) indicates the cross-linking of CIPPO, and there are two protons in the methylene bridge, therefore, CLD should be half of AP at position *e*. CLD can therefore be calculated by eq. (10)

$$CLD(\%) = \frac{0.5A(H_e)}{0.5A(H_a)+A(H_d)+0.5A(H_{d'})} \times 100 \quad (10)$$

It can be observed that AP at position e should be the same as that at position d' , i.e., $A(H_e)$ equals to $A(H_{d'})$. Thus, $A(H_d)$ equals to $(A(H_d, H_{d'}) - 0.5A(H_e))$. Due to the same chemical shift of protons at positions d and d' , the eq. (10) can be converted as eq. (11).

$$CLD(\%) = \frac{0.5A(H_e)}{0.5A(H_a)+A(H_d, H_{d'})+0.5A(H_e)} \times 100 \quad (11)$$

Therefore, if eq. (7) is used to calculate the degree of chloromethylation, i.e., DC_I , the cross-linking was not taken into consideration, thus, the result should be inaccurate and higher than the actual one. This might be the main reason resulting in the differences of $A(H_d)/A(H_c)$ between the theoretical and calculated values in table S1. As a result, the alkylation reaction would not only produce the cross-linked structure with a methylene bridge, but also give a higher DC value if eq. (7) was used. This might explain the earlier observation in the introduction, i.e., the membrane with a high degree of chloromethylation shows low ionic conductivity. As for eq. (8), the protons at position a are not considered and this will cause an overestimate of DC .

As is shown in table S1, the reaction conditions have a significant effect on DC_2 and CLD . The details were studied and analysed in the supplementary information. When other reaction conditions are fixed, a high ratio/concentration of catalyst is more beneficial for chloromethylation at low temperatures, while long reaction time and high temperature facilitate cross-linking. Finding a suitable range for DC_2 and CLD not only has a significant influence on the membrane preparation process, but also largely determines the properties of anion exchange membranes. When the degree of cross-linking is high (>4.8%), the polymer becomes insoluble in chloroform and after filtration. No NMR signal of the polymer could be detected.

In order to ensure the solubility in NMP during quaternisation process, CIPPO polymers with the DC_2 higher than 29.5% and CLD lower than 4.8% were found to be suitable for quaternisation and membrane processing. The studies on the quaternisation process were shown in the supplementary information.

3.4 Morphology

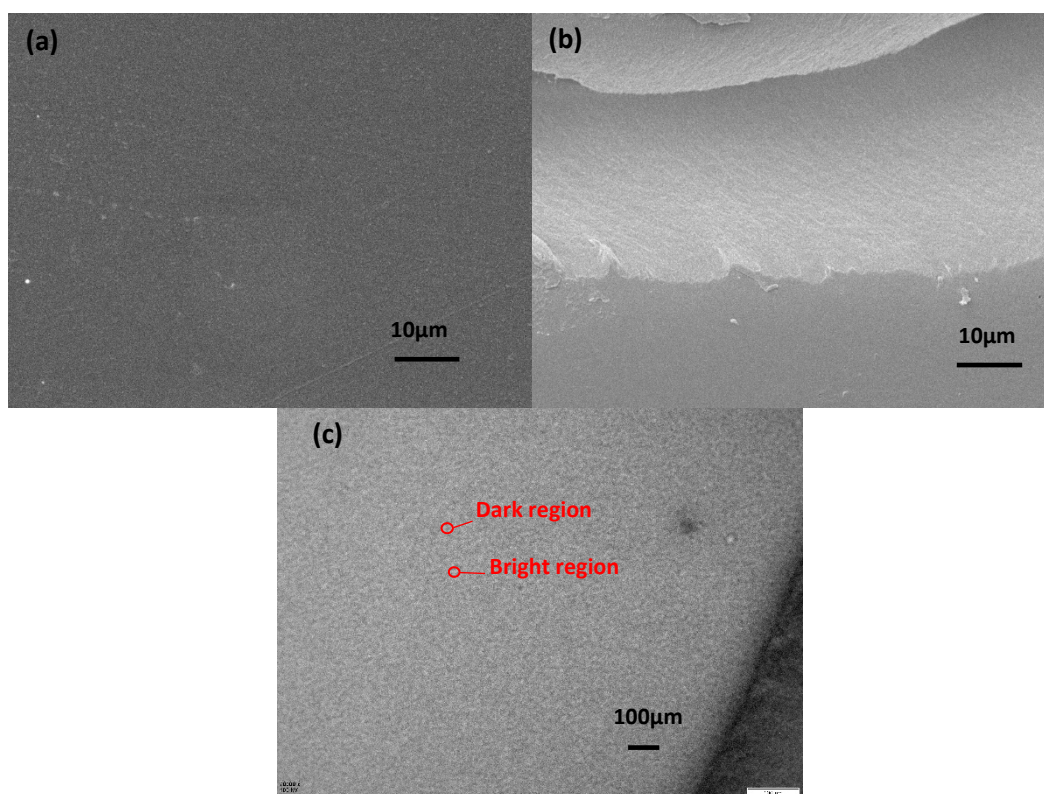


Fig. 5. The SEM images of (a) surface and (b) cross-section of QPPO-14 (dry, thickness 110 μm). (c) The TEM image of the QPPO-14 membrane stained with tetrachloroplatinate ions.

The SEM images of surface and cross-section are shown in Fig. 5(a) and (b). A uniform and smooth structure can be observed. The membrane is homogeneous and sense.[33, 52] The TEM image was shown in Fig. 5(c). in which the phase separation was observed.[53] The dark and bright regions represent the hydrophilic and hydrophobic domains, respectively.[54]

3.5 Thermal stability

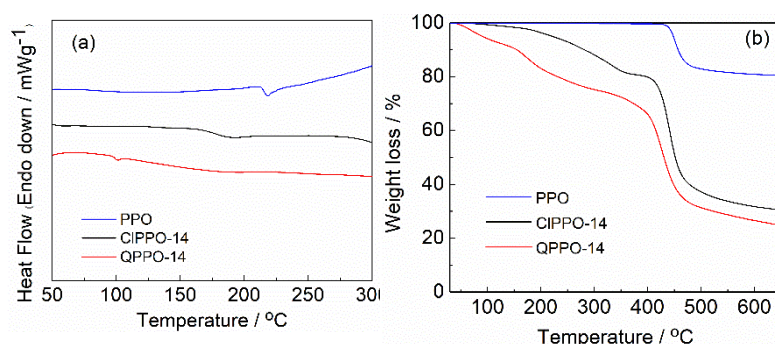
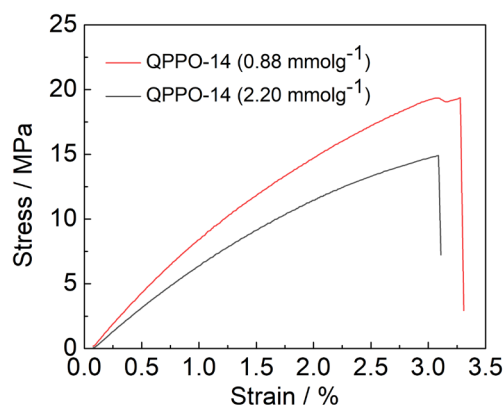


Fig. 6. (a) The DSC and (b) TGA curves of pure PPO, CIPPO-14 and QPPO-14.

Thermal stability of the functionalized polymer is also an important property of AEMs and thus DSC and TGA were used to study QPPO thermal properties. Fig. 6(a) and (b) shows the DSC and TGA curves of PPO, CIPPO and QPPO. CIPPO exhibits a clear glass transition temperature around 160 °C. The glass transition temperature (T_g) of PPO polymer is at 210 °C. For TGA, there is only one degradation step at 430 °C, indicating the high thermal stability. The data are in accordance with the results reported in the papers [55-57]. For QPPO, there is a small endothermic peak at 100 °C, which is caused by the vaporisation of residual water from inside the membranes. As is shown in table S4, for TGA curves, the QPPO AEM exhibits a small mass loss (<5%) below the temperature of 150 °C, which is attributed to inner water loss from the polymer [58]. As discussed earlier that QPPO shows good water uptake. Even the membranes were fully dried in a vacuum oven at 60 °C before the thermal stability tests, the QPPO rapidly absorbed water from the air during sample transfer to the TGA instrument. The onset decomposition seen at 170 °C in QPPO is due to the degradation of the head group [59]. Finally, the second stage weight loss occurs around 400 °C can be assigned to backbone chain decomposition.

3.6 Mechanical Properties



Mechanical properties of QPPO-14 with different *IEC* were tested at room temperature. The membranes in hydroxide form were submerged in water for 1 h before testing. As is shown in Fig. 7, QPPO-14 was chosen owing to the suitable degree of chloromethylation and its potential application in water electrolyser. The stress of break and elongation of QPPO-14 (2.20 mmol g⁻¹) is above 12 MPa and 3 % respectively, which is in agreement with the values reported by Wu and co-workers (17 MPa and 3.5 %, shown in table 1) for similar *IEC* membrane (2.10 mmol g⁻¹) but with QPPO-14 exhibiting over 7 folds increase in ionic conductivity and water uptake [42]. As expected in comparison to lower *IEC* reported QPPO membrane (table 3, 1.0 mmol g⁻¹) [34]. QPPO-14 (2.20 mmol g⁻¹) shows an order of magnitude lower elongation at break and half the ultimate tensile strength, due to high *IEC* and high swelling up but over 8 folds higher conductivity and water uptake.

A comparison of membrane properties among ion exchange membranes based on varieties of backbones was shown in table 1. In comparison to QPO-A which was also prepared via Friedel-Crafts reaction by using different chloromethylation reagents [42], QPPO shows a higher ionic conductivity and higher *IEC*. Besides, compared with radiation grafted low-

density polyethylene with vinylbenzyl chloride functionalised with TMA (LDPE-g-VBC-TMA) [41], QPPO shows the same level of ionic conductivity but a much higher ultimate tensile strength. QPPO-A and QPPO-B were also prepared by using Friedel-Crafts reaction but with different chloromethylation reagents, exhibiting a much lower *IEC* and ionic conductivity [34, 42]. As is shown in table 1, compared with LDPE-g-VBC-TMA [17, 41], QPPO exhibits higher tensile strength owing to the rigid aromatic structure in the backbone. Compared with the commercial AEMs FAA3, QPPO shows lower ultimate tensile strength [23]. Reinforcement of the membrane by pore filling or fibre integration can be done to improve further the mechanical properties of the QPPO based membrane. When compared with Nafion 212 [41, 60], QPPO demonstrates higher ultimate tensile strength despite having more than double the *IEC*. Different from the linear perfluorosulfonic structure of Nafion 212, QPPO in this work shows high water uptake (WU) which inevitably increases the swell ratio (SR) and thickness. The cross-linking structure prevents further expansion of the molecular chain when more water molecules gather near the functional groups.

Table 1. The properties of different membranes at room temperature.

Sample	<i>IEC</i> ^a (mmol g ⁻¹)	Thickness (wet, μm)	σ (mS cm ⁻¹)	<i>WU</i> (wt %)	<i>SR</i> ^d (wt %)	Ultimate tensile strength (MPa)	Elongation at break (%)
QPPO-14 (this work)	2.20	160	58.3	430	49	14	3.1
QPPO-A [42]	2.1	151	7.9	24	– ^e	17	4.3
LDPE-g-VBC-TMA [17, 41]	2.3	96 & 120	54	254	38.8	2.4	41
Nafion 212 [41, 60]	0.91	51	77.4 ^{bc}	14.93	39.6	9	85
QPPO-B [34]	1	–	7	26.4	–	28.8	43.4
Fumasep [®] FAA3 [23]	1.7-2.1	25-35	40	-	2(Br)	40	20-40

^aIEC is mmol Cl⁻ per gram. ^bThe conductivity was tested at 30 °C. ^cThe ionic conductivity of Nafion 212 was proton conductivity. ^dThe length changes were measured. ^e– means no data obtained.

3.7 IEC, Ionic conductivity, water uptake and swelling ratio

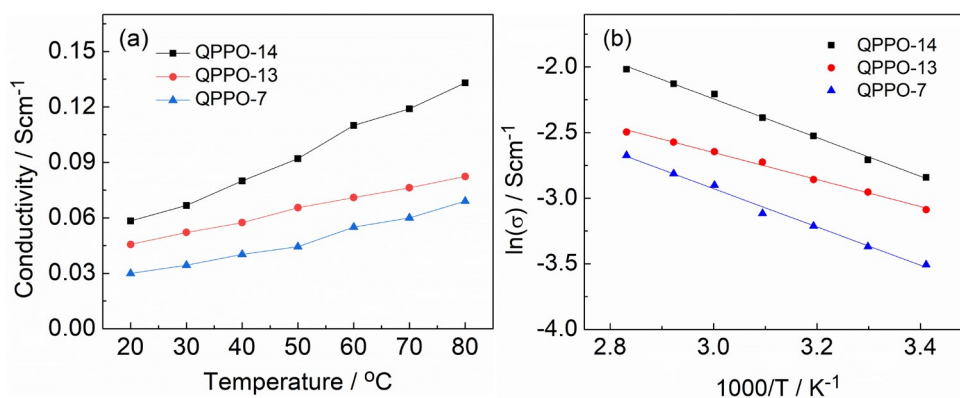


Fig. 8. (a) Ionic conductivity of membranes with different *IEC* as a function of temperature. (b) The Arrhenius-type temperature plots.

Ionic conductivity is another important property to evaluate the ability of AEMs to transfer hydroxide ions and consequently affecting IR loss in water electrolyser. The ionic conductivity and activation energy were calculated by using eq. 5 and eq. 6, respectively. Fig. 8(a) shows the through-plane conductivity of different membranes. QPPO-14 (2.20 mmol g⁻¹), QPPO-13 (2.01 mmol g⁻¹) and QPPO-7 (1.75 mmol g⁻¹) were tested from room temperature to 80 °C. All these three membranes showed an increase in conductivity with the increase of temperature to 80 °C. As expected, membranes with higher IEC and large channels for water transportation display higher conductivity at the same temperature. For example, at 20 °C, the ion conductivity of QPPO-14 is around 0.058 S cm⁻¹, which is higher than that of QPPO-13 (0.045 S cm⁻¹) and QPPO-7 (0.027 S cm⁻¹). QPPO-14 exhibited one of the highest ionic conductivity (0.133 S cm⁻¹ at 80 °C) in comparison to other reported PPO-based membranes in the literature (with a higher degree of chloromethylation also prepared via Friedel-Crafts reaction) [29, 31-34]. The ionic conductivity at elevated temperature was also presented as the Arrhenius plot. Ion conduction is facilitated when the activation energy is low. As is shown in Fig. 8(b), the OH⁻ conductivity shows an approximate exponential temperature dependence [61]. The relationship between ionic conductivity and temperature follows the

Arrhenius equation. Active energy (E_a) is the minimum energy required for the chemical reaction. The lower the E_a , the lower the energy barrier for hydroxide transport [62, 63]. The E_a values of QPPO-14, QPPO-13 and QPPO-7 are 12.26, 8.53 and 12.13 KJ mol⁻¹, respectively, lower than that reported for other AEMs (18 KJ mol⁻¹) [64, 65]. This suggests there is rapid hydroxide transport in prepared QPPO AEMs [65-67]. QPPO-13 exhibited the lowest E_a value, which suggests the facile transport of OH⁻ ions through ion channels which can be attributed to higher water uptake. The crosslinking degree of QPPO-13 is lower than that of QPPO-14 and QPPO-7 (see table S1 in supplementary data). The tight crosslinking structure of QPPO-14 and QPPO-7 will result in lower water uptake causing an adverse effect on the ionic conductivity [68, 69].

The water uptake and the swelling ratio were shown in table 1. The swelling up occurs in all directions, including length, width and thickness. It is not difficult to observe that the water uptake is quite high for QPPO while that of Nafion is low. This might be due to the higher molecular weight for Nafion in comparison with H₂O since Nafion is perfluorosulfonic acid membrane and the *IEC* of Nafion is relatively low. When absorbing the same amount of water, Nafion will show lower water uptake. But for PPO, the molecular weight is quite low, thus the water uptake is quite high. The high water uptake was also observed for the LDPE membrane [41].

3.8 Alkaline stability

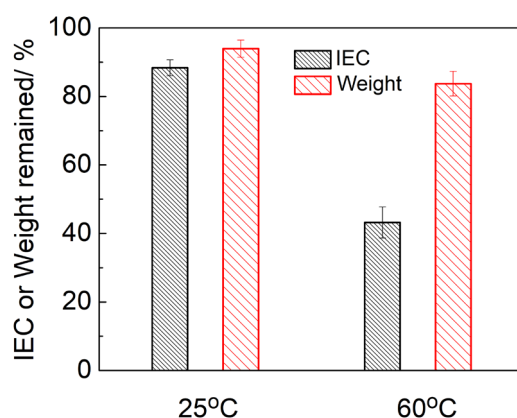


Fig. 9. *IEC* and weight remained of QPPO-14 (2.20 mmol g^{-1}) after immersing in 1 M KOH at 25 °C and 60 °C for 500 h.

AEMs need to have good chemical stability for the long-term application in water electrolyser. The *IEC* and weight change of QPPO-14 (2.20 mmol g^{-1}) were measured after immersion in 1M KOH at 25 °C and 60 °C for 500 h. *IEC* and the weight of the samples were measured. As is shown in Fig. 9, temperature has a vital influence on degradation. The aged QPPO-14 retained >88 % of its *IEC* and > 94% of its original mass at 25 °C after 500 h. On the other hand, at 60 °C, PPO-14 retained only 43 % of its *IEC* but 84% of its original mass, suggesting that most of the degradation is affecting the head group instead of the backbone. This might result from steric hindrance[70, 71]. The cross-linking structure and the methyl groups around the ether bond might protect the backbone from the attack from the OH^- . Besides, the decrease for the *IEC* is expected from alkaline degradation involving the TMA head group. As reported in the literature [41, 72], TMA is a good leaving group and the degradation is mainly due to the OH^- attack on the TMA cation group via nucleophilic substitution in a high alkaline environment ($\text{pH}>13$). Benzylic alcohol is produced consequently. Stevens rearrangement for the benzyl-TMA group is also a minor decomposition route [73], in which process, a ylide intermediate is formed firstly and then a

tertiary amine and water are produced finally. In our tests, we aim to use low concentration alkaline supporting electrolyte of 0.1M and ideally deionised as of PEMWE systems. We will be dedicating separate research articles on detailed understanding and study of degradation of PPO based AEM in an environment relevant to water electrolyser [74].

As is shown in table 2, QPPO based membrane showed 67 % loss of IEC, higher than that of the uncrosslinked QPPO based membrane (40 % loss of IEC) [75], because QPPO based membrane had higher IEC and suffered more attack from OH⁻ ions [57]. Compared with the other types of membranes [76-79], QPPO based membranes showed poor alkaline stability. There are two main reasons. On the one hand, the ionic conductivity of other membranes is much lower than QPPO based membranes, which decreases the possibility of losing the functional group. On the other hand, compared with other functional groups, for instance, the imidazole group (Im) [80], benzyl ammonium has relatively low alkaline stability. Therefore, the membrane needs to be reinforced in future work to protect the functional group.

Table 2. Alkaline stability comparison of reported membranes.

Sample	IEC (mmol g ⁻¹)	σ (mS cm ⁻¹)	Testing condition	Stability result	Ref
QPPO	2.2	59 (20 °C)	1 M KOH at 60 °C for 500 h	67 % loss of IEC	This work
Uncrosslinked QPPO	1.78	-	1 M KOH at 60 °C for 30 days	40 % loss of IEC	[75]
QMter-co-Mpi-100%	2.42	35 (30 °C)	1 M KOH at 60 °C for 500 h	3.3 % loss of IEC	[78]
PES-Im-38	1.86	57.6 (80 °C)	1 M KOH at 60 °C for 168 h	7.5 % loss of IEC	[80]
MBPES	2.03	105 (80 °C)	1 M KOH at 60 °C for 200 h	10.8 % loss of IEC	[76]
QAPS-OH	1.34	18 (30°C)	1 M NaOH at 60 °C 342 h	5.2 % loss of IEC	[77]

3.9 Electrolysis test

The electrochemical performance of the membranes and the ionomers were tested in electrolyser cells by preparing a membrane electrolyte assembly (MEA) using Pt/C catalyst at the cathode (0.4 mg cm^{-2}) and NiCo_2O_4 at the anode (2 mg cm^{-2}) [17]. The active area is 1 cm^2 . The performance was recorded through steady state linear sweep voltammetry at a scan rate of 1 mVs^{-1} between 1.3 and 2V in 0.1 M NaOH at $40 \text{ }^\circ\text{C}$ [14]. In this paper, QPPO-14 (2.20 mmol g^{-1}) was used as both membrane (M, $160 \text{ }\mu\text{m}$) and ionomer (I) due to the consideration of ionic conductivity and compatibility between the membrane and ionomer. Using the same QPPO, the membranes and the ionomer will have similar properties, which offers better contact in the interface and reduces the contact resistance. The test was benchmarked against radiation grafted low-density polyethylene (LDPE) AEM membrane (2.30 mmol g^{-1} , $120\mu\text{m}$) reported elsewhere [72]. The PPO based ionomer was also benchmarked against uncross-linked quaternised polystyrene-*b*-poly(ethylene/butylene)-*b*-polystyrene (SEBS) (1.9 mmol g^{-1}) ionomer with bulky ionic clusters (60% wt styrene) reported elsewhere [17]. Despite QPPO-14 having higher *IEC* than SEBS based ionomer, its rigid structure, *CLD* of 3.8% and lower SR, results in significantly lower ionic conductivity at $40 \text{ }^\circ\text{C}$ of $0.08 \text{ vs. } 0.13 \text{ S cm}^{-1}$ for SEBS [17]. The lower swelling ratio, while desired for membrane mechanical stability, is expected to show slower water permeation through the membrane/ionomer, a critical factor for superior AEM performance [81]. Fig. 10(a) shows the comparison of the electrolyser performances by using the different combinations of membrane and ionomer. Their corresponding impedance data are shown in Fig. 10(b). The electrolyser with the combination of PPO membrane and SEBS ionomer performed lower compared to the other three electrolyser samples over the full testing voltage range. To obtain the current density of 100 mA cm^{-2} with supporting electrolyte of 0.1 M NaOH at $40 \text{ }^\circ\text{C}$, cell

voltage for M_{LDPE-I}PPO, M_{LDPE-I}SEBS, M_{PPO-I}PPO, and M_{PPO-I}SEBS electrolyzers were 1.74 V, 1.73 V, 1.74 V and 1.77 V, respectively. At 1.75V, the current density of the four different combination of membranes and ionomers were 102 mAcm⁻² (M_{LDPE-I}PPO), 127 mAcm⁻² (M_{LDPE-I}SEBS), 120 mAcm⁻² (M_{PPO-I}PPO) and 73 mAcm⁻² (M_{PPO-I}SEBS), respectively. There was small difference in the performance of M_{LDPE-I}PPO, M_{LDPE-I}SEBS and M_{PPO-I}PPO samples in comparison to that of M_{LDPE-I}SEBS. At the studied conditions of low concentration of supporting electrolyte (pH 13), ionomer conductivity plays important role in catalyst layer utilisation and electrolyzer performance. Equally, the interaction of ionomer-membrane and membrane mechanical properties is equally important. Both the chemical and mechanical compatibility between ionomer and membrane will affect significantly the contact resistance and area specific resistance (ASR). Membrane mechanical properties will also affect indirectly the catalyst layer performance. Softer membranes with lower tensile strength will result in better contact of catalyst layer with membrane resulting in lower contact resistance and improved catalyst layer utilisation. However, soft membranes with low tensile strength will suffer from faster failure. Softer membranes will be compressed and become thin under compression while initially resulting in lower area specific resistance this will eventually result in a short circuit with time. For example, the LDPE membrane showed failure after 50 h of operation [17, 82]. Compared with LDPE-based membrane [83], PPO-based membrane is more rigid due to the high content of aromatic rings in the backbones, which will cause less shape and thickness changes, in agreement with mechanical properties testing shown and discussed in table 3 above. The changes in the area specific resistance calculated from the impedance at the cell voltage of 1.7 V are shown in table S5. ASR for four the studied samples were 116 mΩ cm⁻² (M_{LDPE-I}PPO), 104 mΩ cm⁻² (M_{PPO-I}PPO), 184 mΩ cm⁻² (M_{PPO-I}SEBS) and 150 mΩ cm⁻² (M_{LDPE-I}SEBS). PPO-based membranes (in combination with PPO ionomer)

showed slightly lower ASR to that of LDPE based AEM which is desired for use in electrolysers despite the higher thickness of PPO membrane in comparison to LDPE based membrane [17]. The lower ASR values for $M_{LDPE-I_{PPO}}$ and $M_{PPO-I_{PPO}}$ in comparison to that of $M_{LDPE-I_{SEBS}}$ and $M_{PPO-I_{SEBS}}$ can be explained by better compatibility between membrane and ionomer resulting in lower contact resistance. On the other hand, the similar chemical and mechanical compatibility between LDPE and SEBS explains the lower ASR of LDPE-SEBS in comparison to that of PPO-SEBS.

As is shown in Fig. 10(b), the charge transfer resistance (CTR) measured at 1.7 V for the $M_{LDPE-I_{PPO}}$, $M_{PPO-I_{PPO}}$, $M_{PPO-I_{SEBS}}$ and $M_{LDPE-I_{SEBS}}$ electrolysers were $1.24 \Omega \text{ cm}^{-2}$, $1.23 \Omega \text{ cm}^{-2}$, $1.71 \Omega \text{ cm}^{-2}$ and $0.92 \Omega \text{ cm}^{-2}$, respectively. This supports the earlier discussion on the effect of ionomer conductivity and water permeability on performance and catalyst utilisation. When using low supporting electrolyte concentration, most ion transport in the catalyst layer occurs via the ionomer. Hence, the most active fraction of the catalyst layer is that adjacent to the membrane which is largely influenced by the good intimate contact and a continuous ionic path between the catalyst layer and the membrane. Importantly, higher conductivity and SR of SEBS in comparison to QPPO ionomer resulted in the seen 26% lower charge transfer resistance when used with the same LDPE membrane. While poor compatibility between QPPO membrane and SEBS ionomer resulted in seen highest charge transfer resistance of $M_{PPO-I_{SEBS}}$ of $1.71 \Omega \text{ cm}^{-2}$. This highlights the importance of ionomer properties and compatibility with membrane on AEM water electrolysis performance at lower voltages and current densities ($< 0.2 \text{ A cm}^{-2}$ and 1.78 V). As current density increases, and membrane IR loss or ASR become more dominant energy loss over kinetic losses, QPPO based membrane AEMWE showed similar performance to that of LDPE based AEMWE despite having 25% higher thickness. This shows the promising potential of using QPPO as an AEMWE

membrane offering lower ASR and SR and consequently lower energy loss and stability towards membrane mechanical failure. Ionomer study reveals the importance of ionomer properties and compatibility with membrane on AEM water electrolysis performance and displays the critical trade-off between ionic conductivity and catalyst utilisation of the ionomer on one hand and SR, rigidity and mechanical properties on the other hand with SEBS based ionomer has superior properties of the former and QPPO the latter.

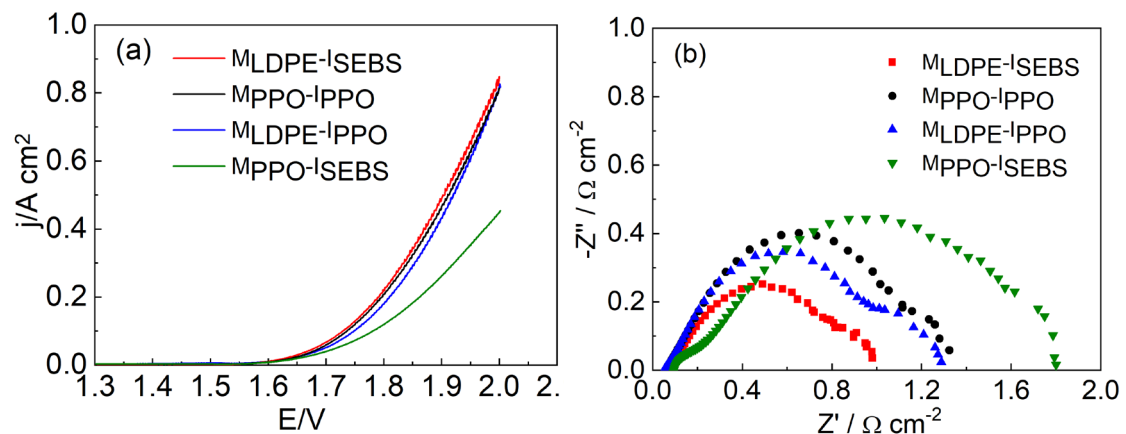


Fig. 10. Polarization curves (a) and corresponding impedance data (b) of different combinations of membrane and ionomer. $M_{LDPE-ISEBS}$ means LDPE as membrane and SEBS as ionomer, $M_{LDPE-IPPO}$ means LDPE as membrane and PPO as ionomer, $M_{LDPE-ISEBS}$ means LDPE as membrane and SEBS as ionomer. $M_{PPO-IPPO}$ means PPO as membrane and ionomer, and $M_{PPO-ISEBS}$ means PPO as membrane and SEBS as ionomer. The tests were conducted in 0.1 M NaOH at 40 °C.

4. Conclusion

Quaternised Poly(2,6-dimethyl-1,4-phenylene oxide) (QPPO) based anion exchange membranes were prepared successfully via Friedel-Crafts reaction using SnCl_4 as catalyst and 1,3,5-trioxane and chlorotrimethylsilane as ‘environmentally friendly’ chloromethylating reagents. The overlooked cross-linking side reaction during the chloromethylation process

was analysed and new equations to calculate the degree of chloromethylation (**DC**) and cross-linking degree (**CLD**) were proposed. QPPO based membrane also showed good mechanical and thermal properties. The stress of break and elongation of QPPO based membranes was found to be above 12 MPa. Alkaline stability tests were conducted in 1M KOH at 25 °C and 60 °C for 500 h, revealing that the main degradation occurred to the functional group rather than the backbone with a 6% loss of **IEC**. QPPO (2.2 mmol g⁻¹) was employed as both membranes and ionomers in electrolyser tests, displaying good electrolysis performance. The area specific resistance for M_{PPPO}-I_{PPPO} electrolysers was as low as 104 mΩ cm⁻² at 40 °C and 0.1M NaOH, and the current density was 814 mAcm⁻² when the potential was 2.0 V. QPPO shows promising potential as AEMWE membrane offering lower ASR and SR and consequently lower energy loss and stability towards membrane mechanical failure.

Acknowledgment

The authors acknowledge the financial support of Newcastle University through the Research Excellence Academy and School of Engineering Ph.D. scholarship scheme to Mr. Zhiming Feng. We also would like to acknowledge the financial support of the British council under Newton Institutional Links fund grant number 261560745 which supported the electrolyser testing work and Spain Ministry of Education, Culture and Sport to fund Prof. Esteban 6 months visit to Newcastle University under PRX17/00183.

References

- [1] Mamlouk M, Manolova M. Chapter 6. Alkaline Anionic Exchange Membrane Water Electrolysers. *Electrochemical Methods for Hydrogen Production* 2019. p. 180-252.
- [2] Abe JO, Popoola API, Ajenifuja E, Popoola OM. Hydrogen energy, economy and storage: Review and recommendation. *Int J Hydrog Energy*. 2019;44:15072-86.
- [3] Li D, Park EJ, Zhu W, Shi Q, Zhou Y, Tian H, et al. Highly quaternized polystyrene ionomers for high performance anion exchange membrane water electrolysers. *Nature Energy*. 2020;5:378-85.
- [4] Gonzalez-Diaz A, Jiang L, Gonzalez-Diaz MO, Roskilly AP, Smallbone AJ. Hydrogen production via ammonia from methane integrated with enhanced oil recovery: A techno-economic analysis. *Journal of Environmental Chemical Engineering*. 2021;9.
- [5] Zakaria K, Thimmappa R, Mamlouk M, Scott K. Hydrogen generation by alcohol reforming in a tandem cell consisting of a coupled fuel cell and electrolyser. *Int J Hydrog Energy*. 2020;45:8107-17.

- [6] Thangavel P, Ha M, Kumaraguru S, Meena A, Singh AN, Harzandi AM, et al. Graphene-nanoplatelets-supported NiFe-MOF: high-efficiency and ultra-stable oxygen electrodes for sustained alkaline anion exchange membrane water electrolysis. *ENERG ENVIRON SCI*. 2020;13:3447-58.
- [7] Dawood F, Anda M, Shafiullah GM. Hydrogen production for energy: An overview. *Int J Hydrog Energy*. 2020;45:3847-69.
- [8] Carmo M, Fritz DL, Mergel J, Stolten D. A comprehensive review on PEM water electrolysis. *Int J Hydrog Energy*. 2013;38:4901-34.
- [9] Liu X, Li Y, Xue J, Zhu W, Zhang J, Yin Y, et al. Magnetic field alignment of stable proton-conducting channels in an electrolyte membrane. *Nat Commun*. 2019;10:842-54.
- [10] Suermann M, Gimpel T, Böhre LV, Schade W, Bensmann B, Hanke-Rauschenbach R. Femtosecond laser-induced surface structuring of the porous transport layers in proton exchange membrane water electrolysis. *J Mater Chem A*. 2020;8:4898-910.
- [11] Zhao Y, Li X, Wang S, Li W, Wang X, Chen S, et al. Proton exchange membranes prepared via atom transfer radical polymerization for proton exchange membrane fuel cell: Recent advances and perspectives. *Int J Hydrog Energy*. 2017;42:30013-28.
- [12] Xing L, Shi W, Su H, Xu Q, Das PK, Mao B, et al. Membrane electrode assemblies for PEM fuel cells: A review of functional graded design and optimization. *Energy*. 2019;177:445-64.
- [13] Wang C, Feng Z, Zhao Y, Li X, Li W, Xie X, et al. Preparation and properties of ion exchange membranes for PEMFC with sulfonic and carboxylic acid groups based on polynorbornenes. *Int J Hydrog Energy*. 2017;42:29988-94.
- [14] Zhao Y, Li X, Li W, Wang Z, Wang S, Xie X, et al. A high-performance membrane electrode assembly for polymer electrolyte membrane fuel cell with poly(arylene ether sulfone) nanofibers as effective membrane reinforcements. *J Power Sources*. 2019;444:227250-8.
- [15] Park HJ, Lee SY, Lee TK, Kim H-J, Lee YM. N3-butyl imidazolium-based anion exchange membranes blended with Poly(vinyl alcohol) for alkaline water electrolysis. *J Membr Sci*. 2020;611:118355.
- [16] Grigoriev SA, Fateev VN, Bessarabov DG, Millet P. Current status, research trends, and challenges in water electrolysis science and technology. *Int J Hydrog Energy*. 2020;45:26036-58.
- [17] Gupta G, Scott K, Mamlouk M. Performance of polyethylene based radiation grafted anion exchange membrane with polystyrene-b-poly (ethylene/butylene)-b-polystyrene based ionomer using NiCo 2 O 4 catalyst for water electrolysis. *J Power Sources*. 2017;375:387-96.
- [18] Gupta G, Selvakumar K, Lakshminarasimhan N, Senthil Kumar SM, Mamlouk M. The effects of morphology, microstructure and mixed-valent states of MnO₂ on the oxygen evolution reaction activity in alkaline anion exchange membrane water electrolysis. *J Power Sources*. 2020;461:228131-42.
- [19] Jasti A, Prakash S, Shahi VK. Stable and hydroxide ion conductive membranes for fuel cell applications: Chloromethylation and amination of poly(ether ether ketone). *J Membr Sci*. 2013;428:470-9.
- [20] He Z, Wang G, Wang C, Guo L, Wei R, Song G, et al. Overview of Anion Exchange Membranes Based on Ring Opening Metathesis Polymerization (ROMP). *Polymer Reviews*. 2021:1-25.
- [21] Li N, Yan T, Li Z, Thurn-Albrecht T, Binder WH. Comb-shaped polymers to enhance hydroxide transport in anion exchange membranes. *ENERG ENVIRON SCI*. 2012;5:7888-92.
- [22] Wang Y, Zhang D, Liang X, Shehzad MA, Xiao X, Zhu Y, et al. Improving fuel cell performance of an anion exchange membrane by terminal pending bis-cations on a flexible side chain. *J Membr Sci*. 2020;595:117483.
- [23] Henkensmeier D, Najibah M, Harms C, Žitka J, Hnát J, Bouzek K. Overview: State-of-the Art Commercial Membranes for Anion Exchange Membrane Water Electrolysis. *J Electrochem Energy Convers Storage*. 2021;18.

- [24] Liu L, Chu X, Liao J, Huang Y, Li Y, Ge Z, et al. Tuning the properties of poly(2,6-dimethyl-1,4-phenylene oxide) anion exchange membranes and their performance in H₂/O₂ fuel cells. *ENERG ENVIRON SCI*. 2018;11:435-46.
- [25] Park AM, Wycisk RJ, Ren X, Turley FE, Pintauro PN. Crosslinked poly(phenylene oxide)-based nanofiber composite membranes for alkaline fuel cells. *J Mater Chem A*. 2016;4:132-41.
- [26] Pan J, Han J, Zhu L, Hickner MA. Cationic Side-Chain Attachment to Poly(Phenylene Oxide) Backbones for Chemically Stable and Conductive Anion Exchange Membranes. *Chem Mater*. 2017;29:5321-30.
- [27] Mohanty AK, Song YE, Jung B, Kim JR, Kim N, Paik H-j. Partially crosslinked comb-shaped PPO-based anion exchange membrane grafted with long alkyl chains: Synthesis, characterization and microbial fuel cell performance. *Int J Hydrog Energy*. 2020;45:27346-58.
- [28] Liu Q, Wang Z, Yu A, Li J, Shen H, Wang H, et al. A novel anion exchange membrane based on poly(2,6-dimethyl-1,4-phenylene oxide) with excellent alkaline stability for AEMFC. *Int J Hydrog Energy*. 2021;46:24328-38.
- [29] Msomi PF, Nonjola P, Ndungu PG, Ramonjta J. Quaternized poly(2,6 dimethyl-1,4 phenylene oxide)/polysulfone blend composite membrane doped with ZnO-nanoparticles for alkaline fuel cells. *J Appl*. 2018;135:45959-67.
- [30] Gopi KH, Bhat SD, Sahu AK, Sridhar P. Quaternized poly(phenylene oxide) anion exchange membrane for alkaline direct methanol fuel cells in KOH-free media. *J Appl*. 2016;133:43693-703.
- [31] Gopi KH, Peera SG, Bhat SD, Sridhar P, Pitchumani S. Preparation and characterization of quaternary ammonium functionalized poly(2,6-dimethyl-1,4-phenylene oxide) as anion exchange membrane for alkaline polymer electrolyte fuel cells. *Int J Hydrog Energy*. 2014;39:2659-68.
- [32] Becerra-Arciniegas RA, Narducci R, Ercolani G, Antonaroli S, Sgreccia E, Pasquini L, et al. Alkaline stability of model anion exchange membranes based on poly(phenylene oxide) (PPO) with grafted quaternary ammonium groups: Influence of the functionalization route. *Polymer*. 2019;185:121931-41.
- [33] Manohar M, Das AK, Shahi VK. Alternative preparative route for efficient and stable anion-exchange membrane for water desalination by electrodialysis. *Desalination*. 2017;413:101-8.
- [34] Arges CG, Wang L, Jung Ms, Ramani V. Mechanically Stable Poly(arylene ether) Anion Exchange Membranes Prepared from Commercially Available Polymers for Alkaline Electrochemical Devices. *J Electrochem Soc*. 2015;162:F686-F93.
- [35] Pantamas N, Khonkeng C. Ecofriendly and Simplified Synthetic Route for Polysulfone-based Solid-State Alkaline Electrolyte Membrane. *Am J Appl Sci*. 2012;9:1577-82.
- [36] Sun Z, Lin B, Yan F. Anion-Exchange Membranes for Alkaline Fuel-Cell Applications: The Effects of Cations. *ChemSusChem*. 2018;11:58-70.
- [37] Galvan V, Shrimant B, Bae C, Prakash GKS. Ionomer Significance in Alkaline Direct Methanol Fuel Cell to Achieve High Power with a Quaternized Poly(terphenylene) Membrane. *ACS Applied Energy Materials*. 2021;4:5858-67.
- [38] Espiritu R, Golding BT, Scott K, Mamlouk M. Degradation of radiation grafted hydroxide anion exchange membrane immersed in neutral pH: removal of vinylbenzyl trimethylammonium hydroxide due to oxidation. *J Mater Chem A*. 2017;5:1248-67.
- [39] Yang J, Yu Q, Zhao F, Lu J, Ge Z. Triacylperhydro-1,3,5-triazines over Phenylsulfonic Acid Functionalized Mesoporous Silica. *Synth Commun*. 2011;41:3455-61.
- [40] Zeng L, He Q, Liao Y, Kuang S, Wang J, Ding W, et al. Anion Exchange Membrane Based on Interpenetrating Polymer Network with Ultrahigh Ion Conductivity and Excellent Stability for Alkaline Fuel Cell. *Research*. 2020;2020:4794706-16.
- [41] Espiritu R, Mamlouk M, Scott K. Study on the effect of the degree of grafting on the performance of polyethylene-based anion exchange membrane for fuel cell application. *Int J Hydrog Energy*. 2016;41:1120-33.

- [42] Wu Y, Wu C, Varcoe JR, Poynton SD, Xu T, Fu Y. Novel silica/poly(2,6-dimethyl-1,4-phenylene oxide) hybrid anion-exchange membranes for alkaline fuel cells: Effect of silica content and the single cell performance. *J Power Sources*. 2010;195:3069-76.
- [43] Wu L, Xu T, Yang W. Fundamental studies of a new series of anion exchange membranes: Membranes prepared through chloroacetylation of poly(2,6-dimethyl-1,4-phenylene oxide) (PPO) followed by quaternary amination. *J Membr Sci*. 2006;286:185-92.
- [44] Lee B, Lim H, Chae JE, Kim H-J, Kim T-H. Physically-crosslinked anion exchange membranes by blending ionic additive into alkyl-substituted quaternized PPO. *J Membr Sci*. 2019;574:33-43.
- [45] A practical and convenient Blanc-type chloromethylation catalyzed by zinc chloride under solvent-free conditions. *Acta Chim Sin*. 2020;78:69-75.
- [46] Gopi KH, Peera SG, Bhat SD, Sridhar P, Pitchumani S. 3-Methyltrimethylammonium poly(2,6-dimethyl-1,4-phenylene oxide) based anion exchange membrane for alkaline polymer electrolyte fuel cells. *Bull Mater Sci*. 2014;37:877-81.
- [47] Gu S, Skovgard J, Yan YS. Engineering the van der Waals interaction in cross-linking-free hydroxide exchange membranes for low swelling and high conductivity. *ChemSusChem*. 2012;5:843-8.
- [48] JONES GD. Chloromethylation of Polystyrene. *Ind Eng Chem Res*. 1952;44:2686-93.
- [49] James AM, Harding S, Robshaw T, Bramall N, Ogden MD, Dawson R. Selective Environmental Remediation of Strontium and Cesium Using Sulfonated Hyper-Cross-Linked Polymers (SHCPs). *ACS Appl Mater Interfaces*. 2019;11:22464-73.
- [50] Al Andis NM. A New Method for Synthesis of Poly(2,6-dimethyl-1,4-phenylene oxide) and Poly(2,6-diphenyl-1,4-phenyl oxide). *J Chem*. 2013;2013:1-4.
- [51] Parrondo J, Jung M-SJ, Wang Z, Arges CG, Ramani V. Synthesis and Alkaline Stability of Solubilized Anion Exchange Membrane Binders Based on Poly(phenylene oxide) Functionalized with Quaternary Ammonium Groups via a Hexyl Spacer. *J Electrochem Soc*. 2015;162:F1236-F42.
- [52] Yu Xu P, Zhou K, Lu Han G, Gen Zhang Q, Mei Zhu A, Lin Liu Q. Fluorene-containing poly(arylene ether sulfone)s as anion exchange membranes for alkaline fuel cells. *J Membr Sci*. 2014;457:29-38.
- [53] Yokota N, Shimada M, Ono H, Akiyama R, Nishino E, Asazawa K, et al. Aromatic Copolymers Containing Ammonium-Functionalized Oligophenylene Moieties as Highly Anion Conductive Membranes. *Macromolecules*. 2014;47:8238-46.
- [54] Hu Y, Wang B, Li X, Chen D, Zhang W. Densely quaternized poly(arylene ether)s with distinct phase separation for highly anion-conductive membranes. *J Power Sources*. 2018;387:33-42.
- [55] Abbasi A, Hosseini S, Somwangthanaroj A, Mohamad AA, Kheawhom S. Poly(2,6-Dimethyl-1,4-Phenylene Oxide)-Based Hydroxide Exchange Separator Membranes for Zinc-Air Battery. *Int J Mol Sci*. 2019;20.
- [56] Lin C-Y, Huang C-H, Hu C-C, Liu Y-L. Self-crosslinkable nitroxide-functionalized poly(2,6-dimethyl-1,4-phenylene oxide) through atom transfer radical coupling reaction. *Polymer*. 2018;135:154-61.
- [57] Dong J, Li H, Ren X, Che X, Yang J, Aili D. Anion exchange membranes of bis-imidazolium cation crosslinked poly(2,6-dimethyl-1,4-phenylene oxide) with enhanced alkaline stability. *Int J Hydrog Energy*. 2019;44:22137-45.
- [58] Lin X, Varcoe JR, Poynton SD, Liang X, Ong AL, Ran J, et al. Alkaline polymer electrolytes containing pendant dimethylimidazolium groups for alkaline membrane fuel cells. *J Mater Chem A*. 2013;1:7262-9.
- [59] Xiao Lin C, Qin Wang X, Ning Hu E, Yang Q, Gen Zhang Q, Mei Zhu A, et al. Quaternized triblock polymer anion exchange membranes with enhanced alkaline stability. *J Membr Sci*. 2017;541:358-66.
- [60] Sherazi TA, Zahoor S, Raza R, Shaikh AJ, Naqvi SAR, Abbas G, et al. Guanidine functionalized radiation induced grafted anion-exchange membranes for solid alkaline fuel cells. *Int J Hydrog Energy*. 2015;40:786-96.

- [61] Tripathi BP, Chakrabarty T, Shahi VK. Highly charged and stable cross-linked 4,4'-bis(4-aminophenoxy)biphenyl-3,3'-disulfonic acid (BAPBDS)-sulfonated poly(ether sulfone) polymer electrolyte membranes impervious to methanol. *J Mater Chem*. 2010;20:8036-44.
- [62] Ma L, Qaisrani NA, Hussain M, Li L, Jia Y, Ma S, et al. Cyclodextrin modified, multication cross-linked high performance anion exchange membranes for fuel cell application. *J Membr Sci*. 2020;607.
- [63] Yang Z, Zhang M, Xiao Y, Zhang X, Fan M. Facile Fabrication of Poly(vinyl alcohol)/Polyquaternium-10 (PVA/PQ-10) Anion Exchange Membrane with Semi-Interpenetrating Network. *Macromolecular Materials and Engineering*. 2020;306.
- [64] Pandey TP, Sarode HN, Yang Y, Yang Y, Vezzù K, Noto VD, et al. A Highly Hydroxide Conductive, Chemically Stable Anion Exchange Membrane, Poly(2,6 dimethyl 1,4 phenylene oxide)-b-Poly(vinyl benzyl trimethyl ammonium), for Electrochemical Applications. *J Electrochem Soc*. 2016;163:H513-H20.
- [65] Shukla G, Shahi VK. Well-designed mono- and di-functionalized comb-shaped poly(2,6-dimethylphenylene oxide) based alkaline stable anion exchange membrane for fuel cells. *Int J Hydrog Energy*. 2018;43:21742-9.
- [66] Gao XL, Sun LX, Wu HY, Zhu ZY, Xiao N, Chen JH, et al. Highly conductive fluorine-based anion exchange membranes with robust alkaline durability. *J Mater Chem A*. 2020;8:13065-76.
- [67] Bai Y, Yuan Y, Miao L, Lü C. Functionalized rGO as covalent crosslinkers for constructing chemically stable polysulfone-based anion exchange membranes with enhanced ion conductivity. *J Membr Sci*. 2019;570-571:481-93.
- [68] Ouadah A, Xu H, Luo T, Gao S, Wang X, Fang Z, et al. A series of poly(butylimidazolium) ionic liquid functionalized copolymers for anion exchange membranes. *J Power Sources*. 2017;371:77-85.
- [69] Li J, Wang S, Liu F, Wang X, Chen H, Mao T, et al. Poly (aryl ether ketone)/polymeric ionic liquid with anisotropic swelling behavior for anion exchange membranes. *J Membr Sci*. 2019;581:303-11.
- [70] Weissbach T, Wright AG, Peckham TJ, Sadeghi Alavijeh A, Pan V, Kjeang E, et al. Simultaneous, Synergistic Control of Ion Exchange Capacity and Cross-Linking of Sterically-Protected Poly(benzimidazolium)s. *Chem Mater*. 2016;28:8060-70.
- [71] Kelly M, Meek CMA, Derek J. Strasser, Zbyslaw R. Owczarczyk, Ami C. Yang-Neyerlin, Bryan S. Pivovar. High-Throughput Anion Exchange Membrane Characterization at NREL. *ECS Transactions*. 2019;92:723-31.
- [72] Espiritu R, Golding BT, Scott K, Mamlouk M. Degradation of radiation grafted anion exchange membranes tethered with different amine functional groups via removal of vinylbenzyl trimethylammonium hydroxide. *J Power Sources*. 2017;375:373-86.
- [73] Arges CG, Ramani V. Two-dimensional NMR spectroscopy reveals cation-triggered backbone degradation in polysulfone-based anion exchange membranes. *Proc Natl Acad Sci U S A*. 2013;110:2490-5.
- [74] Bhushan M, Mani M, Singh AK, Panda AB, Shahi VK. Self-standing polyaniline membrane containing quaternary ammonium groups loaded with hollow spherical NiCo₂O₄ electrocatalyst for alkaline water electrolyser. *J Mater Chem A*. 2020.
- [75] Parrondo J, Wang Z, Jung MS, Ramani V. Reactive oxygen species accelerate degradation of anion exchange membranes based on polyphenylene oxide in alkaline environments. *Phys Chem Chem Phys*. 2016;18:19705-12.
- [76] Shen B, Sana B, Pu H. Multi-block poly(ether sulfone) for anion exchange membranes with long side chains densely terminated by piperidinium. *J Membr Sci*. 2020;615.
- [77] Yang C, Wang S, Ma W, Jiang L, Sun G. Comparison of alkaline stability of quaternary ammonium- and 1,2-methylimidazolium-based alkaline anion exchange membranes. *J Membr Sci*. 2015;487:12-8.
- [78] Yan X, Yang X, Su X, Gao L, Zhao J, Hu L, et al. Twisted ether-free polymer based alkaline membrane for high-performance water electrolysis. *J Power Sources*. 2020;480.

- [79] Cheng C, He X, Huang S, Zhang F, Guo Y, Wen Y, et al. Novel self-cross-linked multi-imidazolium cations long flexible side chains triblock copolymer anion exchange membrane based on ROMP-type polybenzonorbornadiene. *Int J Hydrog Energy*. 2020;45:19676-90.
- [80] Shen B, Pu H. Poly(ether sulfone)s with pendent imidazolium for anion exchange membranes via click chemistry. *Polymer*. 2020;207.
- [81] Mamlouk M, Horsfall JA, Williams C, Scott K. Radiation grafted membranes for superior anion exchange polymer membrane fuel cells performance. *Int J Hydrog Energy*. 2012;37:11912-20.
- [82] Gupta G, Scott K, Mamlouk M. Soluble Polystyrene-b-poly (ethylene/butylene)-b-polystyrene Based Ionomer for Anion Exchange Membrane Fuel Cells Operating at 70 °C. *Fuel Cells*. 2018;18:137-47.
- [83] Mamlouk M, Scott K. A boron phosphate-phosphoric acid composite membrane for medium temperature proton exchange membrane fuel cells. *J Power Sources*. 2015;286:290-8.